Advances in Nano Research, *Vol. 11, No. 5 (2021) 537-546*
https://doi.org/10.12989/anr.2021.11.5.537

Dynamic analysis of quadrilateral concrete foundation integrated with NFRP layers based on numerical method

Mahdi Mahjoobi, Mahmood Rabani Bidgoli* and Hamid Mazaheri

Department of Civil Engineering, Khomein Branch, Islamic Azad University, Khomein, Iran

(*Received March 29, 2021, Revised October 3, 2021, Accepted October 10, 2021*)

Abstract. Mathematical modelling of quadrilateral concrete foundation is a novel topic in the literature. In this paper, dynamic response of quadrilateral concrete foundation resting on soil medium subjected to blast load is presented for the first time. The concrete foundation is covered by nano-fiber reinforced polymer (NFRP) layers at the top and bottom surfaces for improving the stiffness. The NFRP are containing carbon nano-fibers (CNF) and its equivalent material characteristics are calculated by Mori-Tanaka model incorporating the agglomeration effects. On the basis of Sinusoidal shear deformation theory (SSDT) and Hamilton's principle, the motion final equations are obtained assuming structural damping utilizing Kelvin-Voigt model. The dynamic deflection of the quadrilateral concrete foundation is discussed based on transformed weighing (TW) coefficients-differential quadrature method (DQM) in conjunction with Newmark method. The influences of different parameters of soil foundation, blast load, volume fraction and agglomeration of CNFs, structural damping, NFRP layer, geometrical parameters and side angles of the quadrilateral concrete foundation are shown on the dynamic displacement. The results are compared with other published works in the literature for presenting the accuracy of the applied model and method. The outcomes show that the dynamic defection will be reduced with enhancing the CNFs volume fraction. In addition, with with increasing the side angle of quadrilateral plate, the dynamic deflection is increased.

Keywords: blast load, dynamic response, NFRP layer, quadrilateral concrete foundation, TW-DQM

1. Introduction

Mechanical behavior analysis of irregular shaped slabs and foundations has been presented in several researches. Zhang *et al*. (2007) presented a new layered quadrilateral flat element for the material and geometric nonlinear finite element analysis of reinforced concrete slab structures. Shao and Wu (2011) investigated the irregular thin plate bending problems on Winkler foundation with the Fourier differential quadrature method. Zhang (2017) achieved the mechanical behavior of laminated CNT-reinforced quadrilateral composite plates subjected to a sudden transverse dynamic load. Guo *et al*. (2018) examined the nonlinear bending of graphene nanoplatelet (GPL) reinforced laminated composite quadrilateral plates using the element-free IMLS-Ritz method. Malveiro *et al*. (2018) studied impact response of damping and track irregularities on the fatigue behaviour of railway deck bridge slab. A novel dynamics model for railway ballastless track with medium-thick slabs was presented by Yang *et al*. (2021). Han *et al*. (2020) studied the dynamic behaviour of an embedded general shape flexible foundation in a transversely isotropic and multilayered half-space. Alhassan *et al*. (2007) offered an approximate analysis for quadrilateral slabs including various cases of aspect ratios and boundary conditions based on actual two-way action. Free vibration of irregular plates via indirect differential quadrature and singular convolution techniques was studied by Ragb *et al*. (2021). Saheed *et al*. (2021) studied the structural behavior of out-of-plane loaded precast lightweight EPS-foam concrete C-shaped slabs.

With respect to the development of the research works in the field of concrete slabs and foundations subjected to blast load, there are several works in the literature in recent years. Ghani Razaghpour *et al*. (2007) presented the response of reinforced concrete slabs reinforced with fiber glass polymer sheets. They used two quantities of 22.4 and 33.4 kg of ANFO explosive material (ANFO) and obtained the Parameters such as the characteristics of blast waves, deflection in the middle of the slab, rebar strain. Experimental tests and three-dimensional numerical analysis were performed by Wu and Chew (2014) to investigate the behavior of multilayer pavements affected by explosions. A series of explosion tests on the bearing capacity of concrete slabs whose aggregates have been replaced by palm particles instead of granite were conducted by Alengaram *et al*. (2016). They used two explosives of 5 and 10 kg of TNT and showed that a concrete slab with palm aggregates under a high explosive load of 10 kg of TNT is not destroyed, while the sample slab without palm aggregates, under this explosive charge was destroyed. Dynamic analysis of inhomogeneous concrete blocks with silica nanoparticles under blast load was performed experimentally and numerically by the Amnieh *et al*. (2018). According to Mindlin's theory, energy method and Hamilton principle, equations of motion were extracted and the weighted differential squares method was

*Corresponding author, Ph.D.,
E-mail: m.rabanibidgoli@gmail.com

ISSN: 2287-237X (Print), 2287-2388 (Online)

used to solve it. They showed that by increasing the discontinuity distance by more than 40 cm, the maximum velocity of the vertical wave propagation does not change. Maheshwari and Naramsetti (2019) provided an accurate solution for investigating the response of machine foundations under random and sinusoidal harmonic explosive loads. They considered three modes to investigate the response of the foundation under the blast load. In the first case, during the explosion, the soil response and maximum displacement remain elastic. In the second case, the explosion is in the elastic state of the structure, but the maximum response is in the plastic state. In the third case, during the explosion, the state of the structure changes from elastic to plastic. Gudžulić *et al*. (2019) studied computational modeling of fiber flow during casting of fresh concrete. Li *et al*. (2020) studied multi-objective design sustainable model for costs of slabs in office buildings. In another research, numerical analysis of fabricated concrete slab subjected to blast load was performed by Zhao *et al*. (2020). Reifatrh *et al*. (2021) investigated the dynamic behavior of externally reinforced RC slabs using FRPs subjected to close-in blast loads numerically and experimentally. Experimental investigation on the structural response of RC slabs subjected to combined fire and blast was offered by Colombo *et al*. (2021). Lee and Kwak (2021) proposed a material model for steel fiber reinforced concrete subjected to dynamic loadings on the basis of an orthotropic concrete model. The effects of strain rate and fiber reinforcement were taken into account in the material model. Huynh *et al*. (2021) presented an strain assumed formulation over polygonal meshes to accurately evaluate the strain fields in damage nonlocal models. Loor *et al*. (2021) calculated buckling and optimization of the rupture beams armed by steel fibers.

To the best of authors' knowledge, the blast analysis of quadrilateral concrete foundation with NFRP layers cannot be found in literature. However, in this paper, dynamic response of viscoelastic quadrilateral concrete foundation with NFRP layers resting on soil foundation subjected to blast load is presented. The core of the sandwich quadrilateral plates is quadrilateral concrete foundation and the facesheets are NFRP layers which are reinforced by CNFs. The viscoelastic property of the structure is taken into account to achieve the realistic simulation based on Kelvin-Voigt model. The RZT is used for accurate simulation and considering the continuity boundary condition between layers. TW-DQM and Newmark methods are applied for solution of the motion equation in order to obtain the dynamic deflection of the sandwich structure. The effect of various parameters such as blast load, soil foundation, structural damping, volume fraction of CNFs, NFRP layer and geometrical parameters of the structure are examined on the dynamic deflection of the structure.

2. Mathematical modeling

Fig. 1 presents a quadrilateral concrete foundation resting on soil medium integrated by NFRP layers with

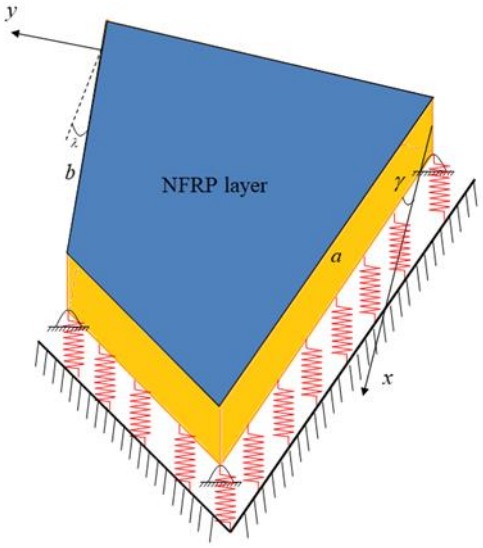

Fig. 1 A quadrilateral concrete foundation with NFRP layers resting on soil foundation

length a, width b, core thickness of h_c, top layer thickness of h_t, bottom layer thickness of h_b and side angles of λ, γ.

Based on the Sinusoidal shear deformation theory, the displacements fields are (Maalla and Song 2021, Hajmohammad et al. 2018)

$$U_1(x,y,z,t) = U(x,y,t) - z\frac{\partial W_b}{\partial x} - \underbrace{\left(z - \frac{\hbar}{\pi} sin\frac{\pi z}{\hbar}\right)}_{f}\frac{\partial W_s}{\partial x}, \quad (1)$$

$$U_2(x,y,z,t) = V(x,y,t) - z\frac{\partial W_b}{\partial y} - \underbrace{\left(z - \frac{\hbar}{\pi} sin\frac{\pi z}{\hbar}\right)}_{f}\frac{\partial W_s}{\partial y}, \quad (2)$$

$$U_3(x,y,z,t) = W_b(x,y,t) + W_s(x,y,t), \quad (3)$$

where U, V and W_b,W_s describe the displacements of mid-plane along x, y and z directions, respectively. The strain-displacements relations may be expressed as

$$\varepsilon_{xx} = \frac{\partial U}{\partial x} - z\frac{\partial^2 W_b}{\partial x^2} - f\frac{\partial^2 W_s}{\partial x^2}, \quad (4)$$

$$\varepsilon_{yy} = \frac{\partial V}{\partial y} - z\frac{\partial^2 W_b}{\partial y^2} - f\frac{\partial^2 W_s}{\partial y^2}, \quad (5)$$

$$\varepsilon_{xy} = \frac{\partial U}{\partial y} + \frac{\partial V}{\partial x} - 2z\frac{\partial^2 W_b}{\partial x \partial y} - 2f\frac{\partial^2 W_s}{\partial x \partial y}, \quad (6)$$

$$\gamma_{yz} = g\frac{\partial W_s}{\partial y}, \quad (7)$$

$$\gamma_{xz} = g\frac{\partial W_s}{\partial x}, \quad (8)$$

where $g = 1 - \frac{df}{dz} = cos(\frac{\pi z}{\hbar})$. The stress-strain equations are

$$\begin{bmatrix}\sigma_{xx}^i\\ \sigma_{yy}^i\\ \sigma_{yz}^i\\ \sigma_{xz}^i\\ \sigma_{xy}^i\end{bmatrix} = \begin{bmatrix}C_{11}^i & C_{12}^i & 0 & 0 & 0\\ C_{21}^i & C_{22}^i & 0 & 0 & 0\\ 0 & 0 & C_{44}^i & 0 & 0\\ 0 & 0 & 0 & C_{55}^i & 0\\ 0 & 0 & 0 & 0 & C_{66}^i\end{bmatrix}\begin{bmatrix}\varepsilon_{xx}^i\\ \varepsilon_{yy}^i\\ \gamma_{yz}^i\\ \gamma_{xz}^i\\ \gamma_{xy}^i\end{bmatrix}, \quad (9)$$

where C_{mn}^i i = t,c,b are elastic constants of the layers. Based on Mori-Tanaka model, the effective elastic modulus (E) and poison's ratio (υ) for the NFRP layers are (Hajmohammad *et al*. 2017, Guo *et al*. 2021)

$$E = \frac{9KG}{3K+G}, \quad (10)$$

$$\upsilon = \frac{3K-2G}{6K+2G}. \quad (11)$$

where the effective bulk modulus (K) and effective shear modulus (G) are defied in Appendix A.

The potential energy of the quadrilateral concrete foundation is

$$\begin{aligned}U = \frac{1}{2}\int_A \Big(&N_{xx}\frac{\partial u}{\partial x} + N_{xy}\frac{\partial u}{\partial y} + N_{xy}\frac{\partial v}{\partial x}\\ &+N_{yy}\frac{\partial v}{\partial y} + Q_x\frac{\partial w_s}{\partial x} + Q_y\frac{\partial w_s}{\partial y} - M_{xxS}\frac{\partial^2 w_s}{\partial x^2}\\ &-M_{yyS}\frac{\partial^2 w_s}{\partial y^2} - 2M_{xyS}\frac{\partial^2 w_s}{\partial y\partial x} - M_{xxB}\frac{\partial^2 w_b}{\partial x^2}\\ &-M_{yyB}\frac{\partial^2 w_b}{\partial y^2} - 2M_{xyB}\frac{\partial^2 w_b}{\partial y\partial x}\Big)dA,\end{aligned} \quad (12)$$

where the resultant forces, moments and transverse shear stresses are

$$\begin{aligned}\left(N_x, N_y, N_{xy}\right) = &\int_{-h_b-h_c/2}^{-h_c/2}\left(\sigma_{xx}^b, \sigma_{yy}^b, \sigma_{xy}^b\right)dz +\\ &\int_{-h_c/2}^{h_c/2}\left(\sigma_{xx}^c, \sigma_{yy}^c, \sigma_{xy}^c\right)dz + \int_{h_c/2}^{h_c/2+h_t}\left(\sigma_{xx}^t, \sigma_{yy}^t, \sigma_{xy}^t\right)dz,\end{aligned} \quad (13)$$

$$\begin{aligned}\left(M_{xxB}, M_{yyB}, M_{xyB}\right) = &\int_{-\hbar_b-\hbar_c/2}^{-\hbar_c/2}\left(\sigma_{xx}^b, \sigma_{yy}^b, \sigma_{xy}^b\right)zdz +\\ &\int_{-\hbar_c/2}^{\hbar_c/2}\left(\sigma_{xx}^c, \sigma_{yy}^c, \sigma_{xy}^c\right)zdz + \int_{\hbar_c/2}^{\hbar_c/2+\hbar_t}\left(\sigma_{xx}^t, \sigma_{yy}^t, \sigma_{xy}^t\right)zdz,\end{aligned} \quad (14)$$

$$\begin{aligned}\left(M_{xxS}, M_{yyS}, M_{xyS}\right) = &\int_{-\hbar_b-\hbar_c/2}^{-\hbar_c/2}\left(\sigma_{xx}^b, \sigma_{yy}^b, \sigma_{xy}^b\right)fdz +\\ &\int_{-\hbar_c/2}^{\hbar_c/2}\left(\sigma_{xx}^c, \sigma_{yy}^c, \sigma_{xy}^c\right)fdz + \int_{\hbar_c/2}^{\hbar_c/2+\hbar_t}\left(\sigma_{xx}^t, \sigma_{yy}^t, \sigma_{xy}^t\right)fdz,\end{aligned} \quad (15)$$

$$\begin{aligned}\left(Q_x, Q_y\right) = &\int_{-\hbar_b-\hbar_c/2}^{-\hbar_c/2}\left(\sigma_{xz}^b, \sigma_{yz}^b\right)dz +\\ &\int_{-\hbar_c/2}^{\hbar_c/2}\left(\sigma_{xz}^c, \sigma_{yz}^c\right)dz + \int_{\hbar_c/2}^{\hbar_c/2+\hbar_t}\left(\sigma_{xz}^t, \sigma_{yz}^t\right)dz,\end{aligned} \quad (16)$$

The kinetic energy of the quadrilateral concrete foundation is

$$K = \frac{1}{2}\rho\int_A\int_{-\frac{h}{2}}^{\frac{h}{2}}\left(\left(\frac{\partial U_1}{\partial t}\right)^2 + \left(\frac{\partial U_2}{\partial t}\right)^2 + \left(\frac{\partial U_3}{\partial t}\right)^2\right)\text{dzdA}. \quad (17)$$

The external works due to the soil medium and blast load may be written as

$$W = -\frac{1}{2}\int_A (q_s + q_b)\, u_3 dA. \quad (18)$$

where the soil medium force is

$$q_v = k_w u_3, \quad (19)$$

in which k_w is the normal spring constant. In addition, the blast force may be given as (Duc *et al*. 2017)

$$q_b = 1.8P_{S0}\left[1 - \frac{t}{T_s}\right]exp\left\{\frac{-at}{T_s}\right\}, \quad (20)$$

where "1.8" is a constant factor, a is wave decay coefficient, P_{S0} is the blast maximum pressure and T_s is the duration parameter for blast pulse which are

$$P_{S0} = 0.085\left(\frac{1}{Z}\right) + 0.3\left(\frac{1}{Z}\right)^2 + 0.8\left(\frac{1}{Z}\right)^3, \quad (21)$$

$$T_s = 1.2\sqrt[6]{W}\sqrt{R}, \quad (22)$$

$$a = Z^2 - 3.7\,Z + 4.2, \quad (23)$$

where P_0 is atmosphere pressure and Z is

$$Z = \frac{R}{W^{0.33}}, \quad (24)$$

where R is the center distance form blast hole to the plate and W is the mass of explosive materials in terms of TNT.

Utilizing Hamilton's principle, the motion equations are

$$\frac{\partial}{\partial x}N_{xx} + \frac{\partial}{\partial y}N_{xy} - I_0\frac{\partial^2 U}{\partial t^2} + I_1\frac{\partial^3 W_b}{\partial x\partial t^2} + J_1\frac{\partial^3 W_s}{\partial x\partial t^2} = 0, \quad (25)$$

$$\frac{\partial}{\partial x}N_{xy} + \frac{\partial}{\partial y}N_{yy} - I_0\frac{\partial^2 V}{\partial t^2} + I_1\frac{\partial^3 W_b}{\partial y\partial t^2} + J_1\frac{\partial^3 W_s}{\partial y\partial t^2} = 0, \quad (26)$$

$$\begin{aligned}&\frac{\partial^2}{\partial x^2}M_{xxB} + 2\frac{\partial^2}{\partial x\partial y}M_{xyB} + \frac{\partial^2}{\partial y^2}M_{yyB} + q\\ &+N_x^m\left(\frac{\partial^2 W_b}{\partial x^2} + \frac{\partial^2 W_s}{\partial x^2}\right) + N_y^m\left(\frac{\partial^2 W_b}{\partial y^2} + \frac{\partial^2 W_s}{\partial y^2}\right)\\ &-I_0\left(\frac{\partial^2 W_b}{\partial t^2} + \frac{\partial^2 W_s}{\partial t^2}\right) - I_1\left(\frac{\partial^3 U}{\partial x\partial t^2} + \frac{\partial^3 V}{\partial y\partial t^2}\right)\\ &+I_2\left(\frac{\partial^4 W_b}{\partial x^2\partial t^2} + \frac{\partial^4 W_b}{\partial y^2\partial t^2}\right) + J_2\left(\frac{\partial^4 W_s}{\partial x^2\partial t^2} + \frac{\partial^4 W_s}{\partial y^2\partial t^2}\right)\\ &= 0,\end{aligned} \quad (27)$$

$$\begin{aligned}&\frac{\partial^2}{\partial x^2}M_{xxS} + 2\frac{\partial^2}{\partial x\partial y}M_{xyS} + \frac{\partial^2}{\partial y^2}M_{yyS} + \frac{\partial}{\partial x}Q_x\\ &+\frac{\partial}{\partial y}Q_y + q\end{aligned} \quad (28)$$

$$
\begin{aligned}
&+ + N_x^m\left(\frac{\partial^2 W_b}{\partial x^2}+\frac{\partial^2 W_s}{\partial x^2}\right)+N_y^m\left(\frac{\partial^2 W_b}{\partial y^2}+\frac{\partial^2 W_s}{\partial y^2}\right)\\
&-I_0\left(\frac{\partial^2 W_b}{\partial t^2}+\frac{\partial^2 W_s}{\partial t^2}\right)-J_1\left(\frac{\partial^3 U}{\partial x\partial t^2}+\frac{\partial^3 V}{\partial y\partial t^2}\right)\\
&+J_2\left(\frac{\partial^4 W_b}{\partial x^2\partial t^2}+\frac{\partial^4 W_b}{\partial y^2\partial t^2}\right)+K_2\left(\frac{\partial^4 W_s}{\partial x^2\partial t^2}+\frac{\partial^4 W_s}{\partial y^2\partial t^2}\right)\\
&=0,
\end{aligned}
$$

where the mass inertias are

$$(I_0, I_1, I_2, J_1, J_1, K_2)=\int_{-\frac{h}{2}}^{\frac{h}{2}}\rho(1, z, f, zf, z^2, f^2)dz. \quad (29)$$

Substituting Eqs. (4)-(9) into Eqs. (13)-(16), assuming structural damping based on Kelvin-Voigt Kolahchi *et al.* (2017) theory ($C_{ij}^k=C_{ij}^k(1+g\partial/\partial t)$) where g is the structural damping coefficient, the stress resultants are

$$
\begin{aligned}
N_x=\left(1+G\frac{\partial}{\partial t}\right)\Bigg[&A_{11}\frac{\partial}{\partial x}U-A_{11z}\frac{\partial^2}{\partial x^2}W_{b_s}\\
&-A_{11f}\frac{\partial^2}{\partial x^2}W\\
&+A_{12}\frac{\partial}{\partial y}V-A_{12z}\frac{\partial^2}{\partial y^2}W_b-A_{12f}\frac{\partial^2}{\partial y^2}W_s\Bigg],
\end{aligned} \quad (30)
$$

$$
\begin{aligned}
N_y=\left(1+G\frac{\partial}{\partial t}\right)\Bigg[&A_{21}\frac{\partial}{\partial x}U-A_{21z}\frac{\partial^2}{\partial x^2}W_b\\
&-A_{21f}\frac{\partial^2}{\partial x^2}W_s\\
&+A_{22}\frac{\partial}{\partial y}V-A_{22z}\frac{\partial^2}{\partial y^2}W_b-A_{22f}\frac{\partial^2}{\partial y^2}W_s\Bigg],
\end{aligned} \quad (31)
$$

$$
\begin{aligned}
N_{xy}=\left(1+G\frac{\partial}{\partial t}\right)\Bigg[&A_{44}\frac{\partial}{\partial y}U+A_{44}\frac{\partial}{\partial x}V\\
&-2A_{44z}\frac{\partial^2}{\partial x\partial y}W_b-2A_{44f}\frac{\partial^2}{\partial x\partial y}W_s\Bigg],
\end{aligned} \quad (32)
$$

$$
\begin{aligned}
M_{xxB}=\left(1+G\frac{\partial}{\partial t}\right)\Bigg[&A_{11z}\frac{\partial}{\partial x}U-B_{11}\frac{\partial^2}{\partial x^2}W_b\\
&-A_{11zf}\frac{\partial^2}{\partial x^2}W_s+A_{12z}\frac{\partial}{\partial y}V-B_{12}\frac{\partial^2}{\partial y^2}W_b\\
&-A_{12zf}\frac{\partial^2}{\partial y^2}W_s\Bigg],
\end{aligned} \quad (33)
$$

$$
\begin{aligned}
M_{yyB}=\left(1+G\frac{\partial}{\partial t}\right)\Bigg[&A_{21z}\frac{\partial}{\partial x}U-B_{21}\frac{\partial^2}{\partial x^2}W_b\\
&-A_{21zf}\frac{\partial^2}{\partial x^2}W_s\\
&+A_{22z}\frac{\partial}{\partial y}V-B_{22}\frac{\partial^2}{\partial y^2}W_b-A_{22zf}\frac{\partial^2}{\partial y^2}W\Bigg],
\end{aligned} \quad (34)
$$

$$
\begin{aligned}
M_{xyB}=\left(1+G\frac{\partial}{\partial t}\right)\Bigg[&2A_{44z}\frac{\partial}{\partial y}U+2A_{44z}\frac{\partial}{\partial x}V\\
&-2B_{44}\frac{\partial^2}{\partial x\partial y}W_b-2A_{44zf}\frac{\partial^2}{\partial x\partial y}W\Bigg],
\end{aligned} \quad (35)
$$

$$
\begin{aligned}
M_{xxS}=\left(1+G\frac{\partial}{\partial t}\right)\Bigg[&A_{11f}\frac{\partial}{\partial x}U-A_{11zf}\frac{\partial^2}{\partial x^2}W_b\\
&-E_{11}\frac{\partial^2}{\partial x^2}W_s\\
&+A_{12f}\frac{\partial}{\partial y}V-A_{12zf}\frac{\partial^2}{\partial y^2}W_b-E_{12}\frac{\partial^2}{\partial y^2}W_s\Bigg]
\end{aligned} \quad (36)
$$

$$
\begin{aligned}
M_{yyS}=\left(1+G\frac{\partial}{\partial t}\right)\Bigg[&A_{21f}\frac{\partial}{\partial x}U-A_{21zf}\frac{\partial^2}{\partial x^2}W_b\\
&-E_{21}\frac{\partial^2}{\partial x^2}W_s\\
&+A_{22f}\frac{\partial}{\partial y}V-A_{22zf}\frac{\partial^2}{\partial y^2}W_b-E_{22}\frac{\partial^2}{\partial y^2}W_s\Bigg],
\end{aligned} \quad (37)
$$

$$
\begin{aligned}
M_{xyS}=\left(1+G\frac{\partial}{\partial t}\right)\Bigg[&2A_{44f}\frac{\partial}{\partial y}U+2A_{44f}\frac{\partial}{\partial x}V\\
&-2A_{44zf}\frac{\partial^2}{\partial x\partial y}W_b-2E_{44}\frac{\partial^2}{\partial x\partial y}W_s\Bigg],
\end{aligned} \quad (38)
$$

$$Q_x=\left(1+G\frac{\partial}{\partial t}\right)\left[A_{55g}\frac{\partial}{\partial x}W_s\right], \quad (39)$$

$$Q_y=\left(1+G\frac{\partial}{\partial t}\right)\left[A_{66g}\frac{\partial}{\partial y}W_s\right], \quad (40)$$

where

$$A_{ij}=\int_{-\hbar_b-\hbar_c/2}^{-\hbar_c/2}C_{ij}^b dz+\int_{-\hbar_c/2}^{\hbar_c/2}C_{ij}^c dz+\int_{\hbar_c/2}^{\hbar_c/2+\hbar_t}C_{ij}^t dz, \quad (41)$$

$$
\begin{aligned}
A_{ijz}=&\int_{-\hbar_b-\hbar_c/2}^{-\hbar_c/2}C_{ij}^b z dz+\int_{-\hbar_c/2}^{\hbar_c/2}C_{ij}^c z dz\\
&+\int_{\hbar_c/2}^{\hbar_c/2+\hbar_t}C_{ij}^t z dz,
\end{aligned} \quad (42)
$$

$$
\begin{aligned}
A_{ijf}=&\int_{-\hbar_b-\hbar_c/2}^{-\hbar_c/2}C_{ij}^b f dz+\int_{-\hbar_c/2}^{\hbar_c/2}C_{ij}^c f dz\\
&+\int_{\hbar_c/2}^{\hbar_c/2+\hbar_t}C_{ij}^t f dz,
\end{aligned} \quad (43)
$$

$$
\begin{aligned}
A_{ijzf}=&\int_{-\hbar_b-\hbar_c/2}^{-\hbar_c/2}C_{ij}^b f z dz+\int_{-\hbar_c/2}^{\hbar_c/2}C_{ij}^c f z dz\\
&+\int_{\hbar_c/2}^{\hbar_c/2+\hbar_t}C_{ij}^t f z dz,
\end{aligned} \quad (44)
$$

$$
\begin{aligned}
B_{ij}=&\int_{-\hbar_b-\hbar_c/2}^{-\hbar_c/2}C_{ij}^b z^2 dz+\int_{-\hbar_c/2}^{\hbar_c/2}C_{ij}^c z^2 dz\\
&+\int_{\hbar_c/2}^{\hbar_c/2+\hbar_t}C_{ij}^t z^2 dz,
\end{aligned} \quad (45)
$$

$$E_{ij} = \int_{-\hbar_b-\hbar_c/2}^{-\hbar_c/2} C_{ij}^{b} f^2 dz + \int_{-\hbar_c/2}^{\hbar_c/2} C_{ij}^{c} f^2 dz + \int_{\hbar_c/2}^{\hbar_c/2+\hbar_t} C_{ij}^{t} f^2 dz, \quad (46)$$

$$A_{ijg} = \int_{-\hbar_b-\hbar_c/2}^{-\hbar_c/2} C_{ij}^{b} dz + \int_{-\hbar_c/2}^{\hbar_c/2} C_{ij}^{c} dz + \int_{\hbar_c/2}^{\hbar_c/2+\hbar_t} C_{ij}^{t} dz, \quad (47)$$

Also, the boundary conditions are assumed as
Clamped supported at four surfaces

$$\begin{aligned} x = 0, a \Rightarrow U = V = W_b = W_s = \frac{\partial W_b}{\partial y} = 0, \\ y = 0, b \Rightarrow U = V = W_b = W_s = \frac{\partial W_b}{\partial x} = 0, \end{aligned} \quad (48)$$

Simply supported at four surfaces

$$\begin{aligned} x = 0, a \Rightarrow U = V = W_b = W_s = M_{yyB} = 0, \\ y = 0, b \Rightarrow U = V = W_b = W_s = M_{xxB} = 0, \end{aligned} \quad (49)$$

Clamped supported at two surfaces and simply supported at two another surfaces

$$\begin{aligned} x = 0, a \Rightarrow U = V = W_b = W_s = \frac{\partial W_b}{\partial y} = 0, \\ y = 0, b \Rightarrow U = V = W_b = W_s = M_{xxB} = 0, \end{aligned} \quad (50)$$

3. TW-DQ methods

In this solution method, the differential equations are translated into a first order algebraic equation by the weighting coefficients. At the first, the material points of the quadrilateral plates in the physical domain (*x*-*y*) should be transformed into the computational domain (*X*-*Y*) of the DQM from the following relations (Kolahchi *et al*. 2017, 2018)

$$\begin{aligned} x = \sum_{i=1}^{4} x_i \, \Phi_i(X, Y), \\ y = \sum_{i=1}^{4} y_i \, \Phi_i(X, Y), \end{aligned} \quad (51)$$

where x_i and y_i are the coordinates of node i in the physical domain, Φ_i is the shape function which is

$$\Phi_i = (-1)^{i+1}(1 - X_i - X)(1 - Y_i - Y) i = 1,2,3,4. \quad (52)$$

Hence, the first- and second-order derivatives from x and y coordinate to X and Y coordinate may be changed as

$$\begin{Bmatrix} \frac{\partial()}{\partial x} \\ \frac{\partial()}{\partial y} \end{Bmatrix} = [T_{11}] \begin{Bmatrix} \frac{\partial()}{\partial X} \\ \frac{\partial()}{\partial Y} \end{Bmatrix}, \begin{Bmatrix} \frac{\partial^2()}{\partial x^2} \\ \frac{\partial^2()}{\partial y^2} \\ \frac{\partial^2()}{\partial x \partial y} \end{Bmatrix} \quad (53)$$

$$= [T_{22}] \begin{Bmatrix} \frac{\partial^2()}{\partial X^2} \\ \frac{\partial^2()}{\partial Y^2} \\ \frac{\partial^2()}{\partial X \partial Y} \end{Bmatrix} + [T_{21}] \begin{Bmatrix} \frac{\partial()}{\partial X} \\ \frac{\partial()}{\partial Y} \end{Bmatrix},$$

where

$$[T_{11}] = \begin{bmatrix} \frac{\partial x}{\partial X} & \frac{\partial y}{\partial X} \\ \frac{\partial x}{\partial Y} & \frac{\partial y}{\partial Y} \end{bmatrix}^{-1},$$

$$[T_{11}] = \begin{bmatrix} \frac{\partial^2 x}{\partial X^2} & \frac{\partial^2 y}{\partial X^2} & \frac{\partial x}{\partial X}\frac{\partial y}{\partial X} \\ \frac{\partial^2 x}{\partial Y^2} & \frac{\partial^2 y}{\partial Y^2} & \frac{\partial x}{\partial Y}\frac{\partial y}{\partial Y} \\ \frac{\partial^2 x}{\partial X \partial Y} & \frac{\partial^2 y}{\partial X \partial Y} & \frac{1}{2}\left(\frac{\partial x}{\partial X}\frac{\partial y}{\partial Y} + \frac{\partial x}{\partial Y}\frac{\partial y}{\partial X}\right) \end{bmatrix} \quad (54)$$

$$[T_{21}] = -[T_{22}][J_{21}][T_{11}], [J_{21}] = \begin{bmatrix} \frac{\partial^2 x}{\partial X^2} & \frac{\partial^2 y}{\partial X^2} \\ \frac{\partial^2 x}{\partial Y^2} & \frac{\partial^2 y}{\partial Y^2} \\ \frac{\partial^2 x}{\partial X \partial Y} & \frac{\partial^2 y}{\partial X \partial Y} \end{bmatrix}.$$

After using above relations, DQM rules should be applied. Hence, the partial derivative of $F(X, Y)$ can be given as

$$\frac{d^n F(X_i, Y_j)}{dX^n} = \sum_{k=1}^{N_X} A_{ik}^{(n)} F(X_k, Y_j) \, n = 1, \ldots, N_X - 1, \quad (55)$$

$$\frac{d^m F(X_k, Y_j)}{dY^m} = \sum_{l=1}^{N_Y} B_{jl}^{(m)} F(X_k, Y_j) \, m = 1, \ldots, N_Y - 1, \quad (56)$$

$$\frac{d^{n+m} F(X_k, Y_j)}{dX^n dY^m} = \sum_{k=1}^{N_X} \sum_{l=1}^{N_Y} A_{ik}^{(n)} B_{jl}^{(m)} F(X_k, Y_j), \quad (57)$$

where $A_{ik}^{(n)}$ and $B_{jl}^{(m)}$ are the weighting coefficients which are:

$$\begin{aligned} A^{(1)}{}_{ij} = \frac{M(X_i)}{(X_i - X_j) M(X_j)}, \\ B^{(1)}{}_{ij} = \frac{P(Y_i)}{(Y_i - Y_j) M(Y_j)}, \end{aligned} \quad (58)$$

where M and P are Lagrangian operators defined as

$$\begin{aligned} M(X_i) = \prod_{j=1}^{N_X} (X_i - X_j), i \neq j \\ P(Y_i) = \prod_{j=1}^{N_Y} (Y_i - Y_j), i \neq j. \end{aligned} \quad (59)$$

Furthermore, N_X and N_Y are the grid point numbers which are

$$X_i = \frac{1}{2}[1 - cos(\frac{\pi i}{N_X})], \\ Y_j = \frac{1}{2}[1 - cos(\frac{\pi j}{N_Y})], \tag{60}$$

Hence, utilizing DQM, the motion final equations are

$$\begin{bmatrix} M_{bb} & M_{bd} \\ M_{db} & M_{dd} \end{bmatrix} \begin{bmatrix} \ddot{Y}_b \\ \ddot{Y}_d \end{bmatrix} + \begin{bmatrix} C_{bb} & C_{bd} \\ C_{db} & C_{dd} \end{bmatrix} \begin{bmatrix} \dot{Y} \\ \dot{Y}_d \end{bmatrix} \\ + \begin{bmatrix} K_{bb} & K_{bd} \\ K_{db} & K_{dd} \end{bmatrix} \begin{bmatrix} Y_b \\ Y_d \end{bmatrix} = \begin{bmatrix} 0 \\ Q_b \end{bmatrix}, \tag{61}$$

in which $[K]$ is stiffness matrix, $[C]$ is the damp matrix, $[M]$ is the mass matrix, $[Q_b]$ is the external blast load, presents, $\{Y\}$) is the displacement vector, subscript b and d indicate the boundary and domain points.

Here, Newmark method (Kolahchi *et al*. 2018) is used to obtain the time response of the structure. Based on this method, Eq. (61) may be given as

$$K^*(d_{i+1}) = Q_{i+1}, \tag{62}$$

where subscript $i+1$ indicates the time $t = t_{i+1}$, $K^*(d_{i+1})$ and Q_{i+1} are the effective stiffness matrix and the effective load vector which are

$$K^*(d_{i+1}) = K_L + K_{NL}(d_{i+1}) + \alpha_0 M + \alpha_1 C, \tag{63}$$

$$Q^*_{i+1} = Q_{i+1} + M(\alpha_0 d_i + \alpha_2 \dot{d}_i + \alpha_3 \ddot{d}_i) \\ + C(\alpha_1 d_i + \alpha_4 \dot{d}_i + \alpha_5 \ddot{d}_i), \tag{64}$$

where

$$\alpha_0 = \frac{1}{\chi \Delta t^2}, \alpha_1 = \frac{\gamma}{\chi \Delta t}, \alpha_2 = \frac{1}{\chi \Delta t}, \\ \alpha_3 = \frac{1}{2\chi} - 1, \alpha_4 = \frac{\gamma}{\chi} - 1, \\ \alpha_5 = \frac{\Delta t}{2}\left(\frac{\gamma}{\chi} - 2\right), \alpha_6 = \Delta t(1-\gamma), \alpha_7 = \Delta t \gamma, \tag{65}$$

in which $\gamma = 0.5$ and $\chi = 0.25$. Based on the iteration method, Eq. (62) is solved at any time step and modified velocity and acceleration vectors are calculated as follows

$$\ddot{d}_{i+1} = \alpha_0(d_{i+1} - d_i) - \alpha_2 \dot{d}_i - \alpha_3 \ddot{d}_i, \tag{66}$$

$$\dot{d}_{i+1} = \dot{d}_i + \alpha_6 \ddot{d}_i + \alpha_7 \ddot{d}_{i+1}, \tag{67}$$

4. Numerical results

In this section, a quadrilateral concrete foundation is assumed with Young's modulus of 20 GPa and Poisson's ratio of 0.3. It is covered by NFRP layer at the top and bottom surfaces considered which is covered by NFRP layers with Young's modulus of 3.5 GPa and Poisson's ratio of 0.33 which is armed by CNFs with Young's modulus of 1 TPa and Poisson's ratio of 0.3.

For validating the results of this study, the NFRP and soil medium are neglected and dynamic response of a plate subjected to blast load is investigated. Assuming the material properties the same as Duc *et al*. (2017), the dynamic displacement is presented in Fig. 2. As may be found, the present outcomes are in good agreement with Duc *et al*. (2017).

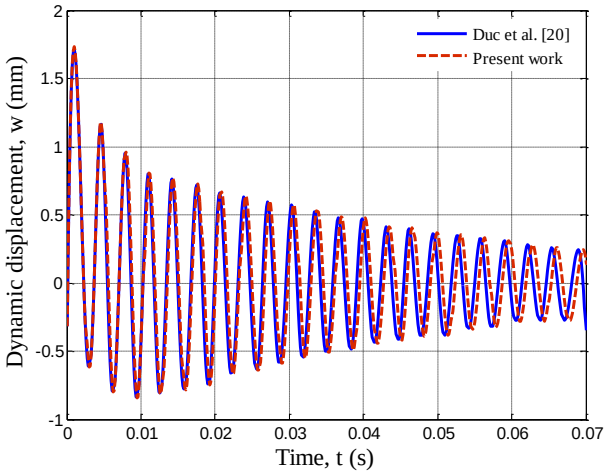

Fig. 2 Comparison of this work with Duc *et al*. (2017)

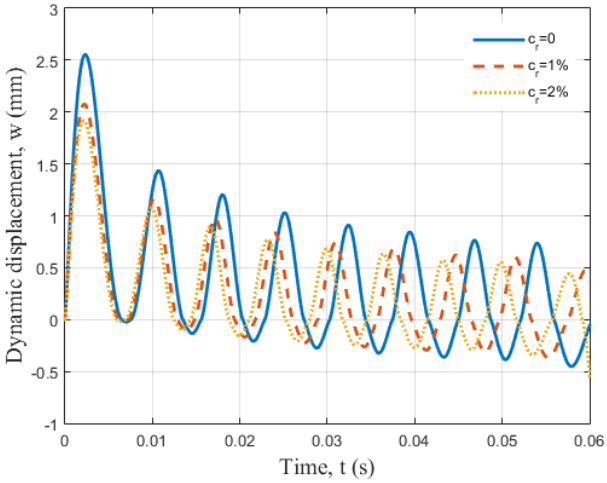

Fig. 3 The influence of CNF volume fraction on the dynamic displacement of the quadrilateral concrete foundation

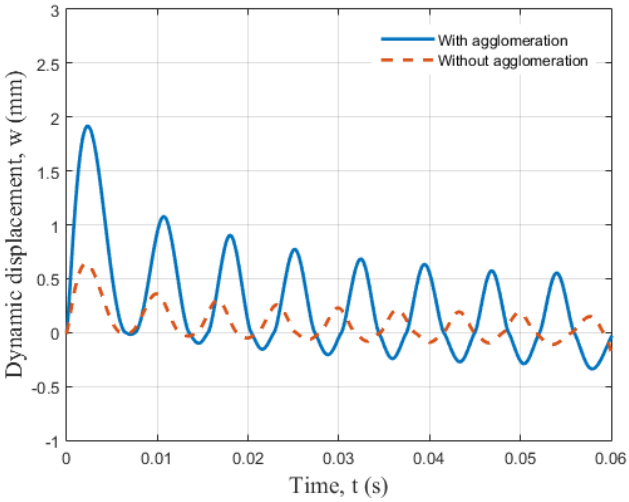

Fig. 4 The influence of the CNFs agglomeration on the dynamic displacement of the quadrilateral concrete foundation

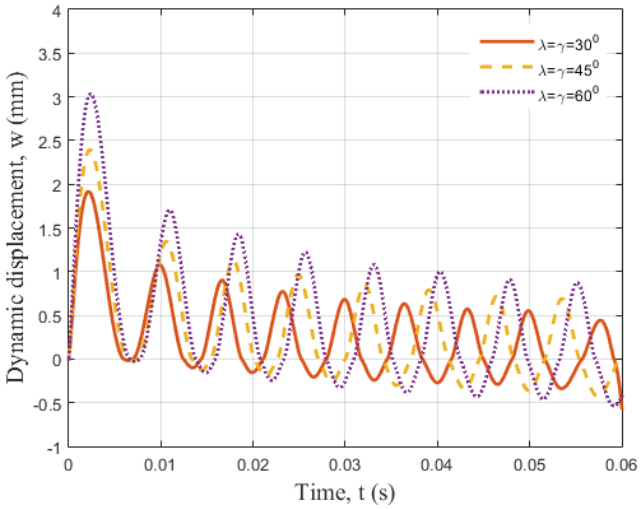

Fig. 5 The influence of the side angle of quadrilateral concrete foundation on the dynamic displacement of the quadrilateral concrete foundation

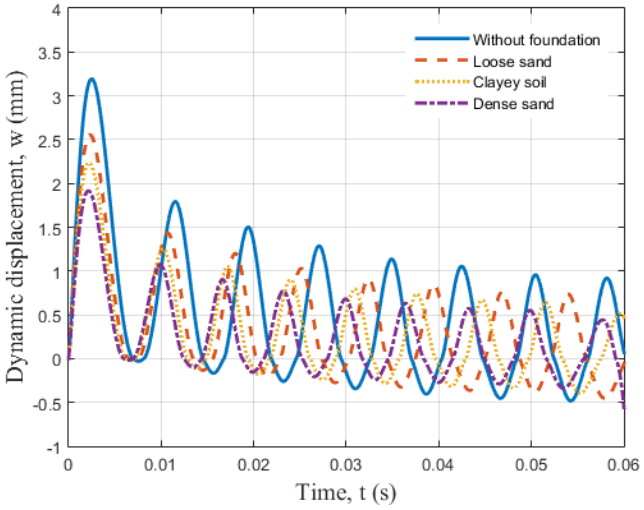

Fig. 6 The influence of the soil medium on the dynamic displacement of the quadrilateral concrete foundation

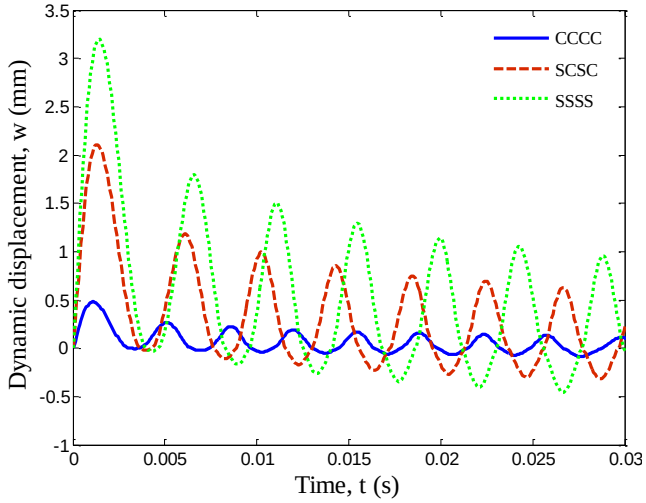

Fig. 7 The influence of the boundary conditions on the dynamic displacement of the quadrilateral concrete foundation

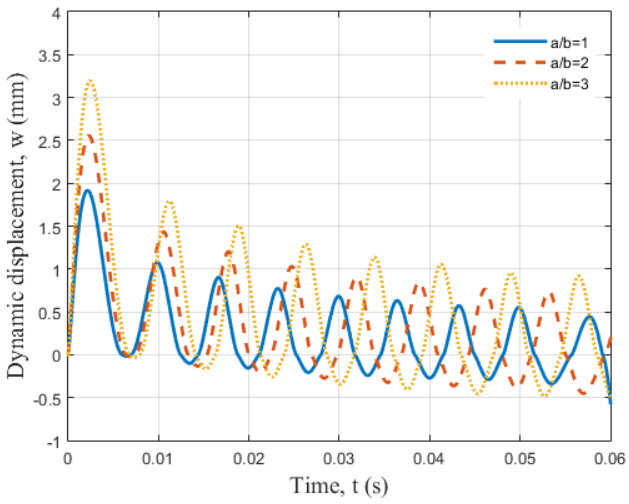

Fig. 8 The influence of the length to width ratio on the dynamic displacement of the quadrilateral concrete foundation

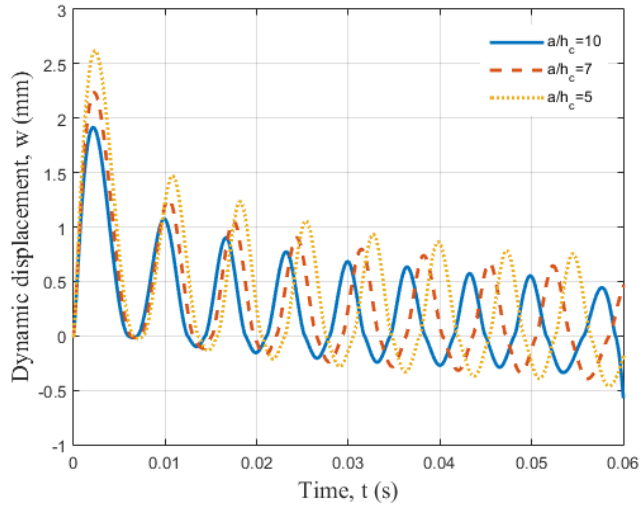

Fig. 9 The influence of the length to total thickness on the dynamic displacement of the quadrilateral concrete foundation

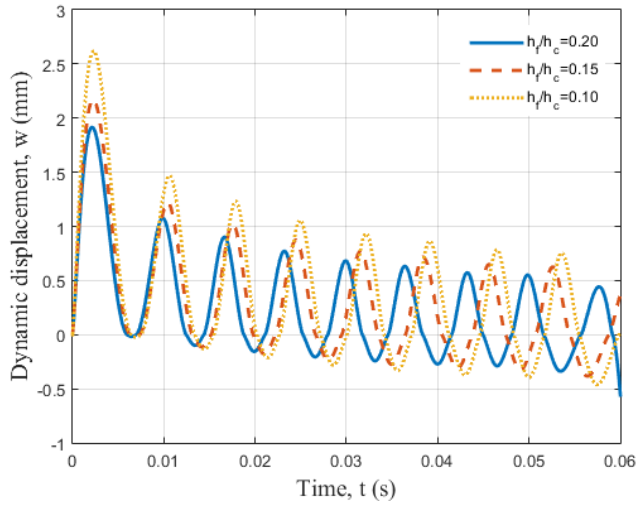

Fig. 10 The influence of the NFRP to core thickness ratio on the dynamic displacement of the quadrilateral concrete foundation

The influence of CNFs volume percent on the dynamic displacement of the quadrilateral concrete foundation is illustrated in Fig. 3. It is found that with reinforcing the structure with CNFs, the dynamic deflection is reduced due to improve the stiffness. In addition, the time of maximum deflection is lower with enhancing the CNFs volume fraction. For quantitative analysis of this figure, the maximum dynamic deflection is 2.58 and 1.88, respectively for without CNFs and face sheets with 2% CNFs. In other words, with reinforcing the NFRP layer with 2% CNFs, the maximum dynamic deflection is reduced about 27%.

Fig. 4 presents the influence of CNFs agglomeration on the dynamic deflection of the quadrilateral concrete foundation. As can be seen, existence of CNFs agglomeration leads to higher dynamic deflection. This effect is considerable on the results so that with considering agglomeration of CNFs, the dynamic deflection is reduced about 66%. This is physically reasonable since with assuming CNFs agglomeration, the stiffness is reduced.

The side angle of quadrilateral concrete foundation on the dynamic deflection is shown in Fig. 5. It can be seen that with enhancing the side angle of quadrilateral concrete foundation, the dynamic deflection is increased. It is due to this fact that with enhancing the side angle of quadrilateral plate concrete foundation the stiffness of is decreased. The influence of soil medium on the dynamic displacement of the quadrilateral concrete foundation is demonstrated in Fig. 6. Here, three cases of loose sand (K_w = 16000 N/m^3), dense sand (K_w = 128000 N/m^3) and Clayey soil (K_w = 80000 N/m^3) are considered. It is observed that with enhancing the soil medium spring constants, the dynamic displacement is reduced. Hence, existence of soil medium leads to more bending rigidity of the quadrilateral concrete foundation under the action of blast load.

The influence of boundary conditions on the dynamic deflection of the quadrilateral concrete foundation is shown in Fig. 7. As can be seen, the dynamic deflection of the quadrilateral concrete foundation with CCCC boundary conditions is minimum with respect to CSCS and SSSS ones since in this case, bending rigidity of the structure is maximum. For example, the dynamic deflection of quadrilateral concrete foundation with CCCC boundary conditions is 0.5 mm while it is 3.25 mm for SSSS ones.

The influences of geometrical parameters of the quadrilateral concrete foundation on the dynamic deflection are studied in Figs. 8-10. Fig. 8 illustrates the influence of length to width ratio of the quadrilateral concrete foundation on the dynamic deflection. It is observed that with enhancing the length to width ratio, the dynamic displacement enhances due to decrease of the stiffness. In Fig. 9, the influence of length to core thickness ratio is presented. As can be seen, with enhancing the length to core thickness ratio, the dynamic displacement is decreased. Fig. 10 presents the influence of NFRP to core thickness ratio on the dynamic displacement. It is found that with enhancing the NFRP to core thickness ratio, the dynamic displacement is reduced due to improve of stiffness.

5. Conclusions

Mathematical modelling of quadrilateral concrete foundation subjected to blast load resting on soil medium was presented in this article based on SSDT. The quadrilateral concrete foundation was covered by nano-fiber reinforced polymer (NFRP) layers at the top and bottom surfaces for improving the stiffness. The Mori-Tanaka model was utilized for obtaining the effective material characteristics of NFRP layers. The motion final equations were derived Hamilton's principle and solved by TW-DQ-Newmark methods. The influences of different parameters of soil foundation, blast load, volume fraction and agglomeration of CNFs, structural damping, NFRP layer, geometrical parameters and side angles of the quadrilateral concrete foundation were shown on the dynamic displacement. The most important findings of this paper were:

• With reinforcing the NFRP layer with 2% CNFs, the maximum dynamic deflection was reduced about 27%.

• The agglomeration effect of CNFs was considerable on the results so that with considering agglomeration of CNFs, the dynamic deflection was reduced about 66%.

• With enhancing the side angle of quadrilateral concrete foundation, the dynamic deflection was increased.

• It was observed that with enhancing the soil medium spring constants, the dynamic displacement is reduced.

• The dynamic deflection of the quadrilateral concrete foundation with CCCC boundary conditions was minimum with respect to CSCS and SSSS ones.

• It was found that with enhancing the NFRP to core thickness ratio, the dynamic displacement is reduced due to improve of stiffness.

References

Alhassan, M.A., Al Rousan, R.Z., Hejazi, M.A. and Amaireh, L.K. (2021), "Approximate analysis of quadrilateral slabs having various cases of boundary conditions and aspect ratios", *Adv. Struct. Eng.*, **24**, 1782-1797. https://doi.org/10.1177/1369433220982099.

Alengaram, U.J., Mohottige, N.H.W., Wu, C., Jumaat, M.Z. and Wang, Z. (2016), "Response of oil palm shell concrete slabs subjected to quasi-static and blast loads, *Constr. Build. Mater.*, **116**, 391-402. https://doi.org/10.1016/j.conbuildmat.2016.04.103.

Amnieh, H.B., Zamzam, M.S. and Kolahchi, R. (2018), "Dynamic analysis of non-homogeneous concrete blocks mixed by SiO_2 nanoparticles subjected to blast load experimentally and theoretically", *Constr. Build. Mater.*, **174**, 633-644. https://doi.org/10.1016/j.conbuildmat.2018.04.140.

Colombo, M., Martinelli, P., Arano, A., Øverli, J.A., Hendriks, M.A.N., Kanstad, T. and Di Prisco, M. (2021), "Experimental investigation on the structural response of RC slabs subjected to combined fire and blast", *Structures*, **31**, 1017-1030. https://doi.org/10.1016/j.istruc.2021.02.029.

Duc, N.D., Seung-Eock, K., Cong, P.H., Anh, N.T. and Khoa, N.D. (2017), "Dynamic response and vibration of composite double curved shallow shells with negative Poisson's ratio in auxetic honeycombs core layer on elastic foundations subjected to blast and damping loads", *Int. J. Mech. Sci.*, **133**, 504-512. https://doi.org/10.1016/j.ijmecsci.2017.09.009.

Ghani Razaghpour, A., Tolba, A. and Contestabile, E. (2007), "Blast loading response of reinforced concrete panels reinforced with externally bonded GFRP laminates", *Soil Dyn. Earthq. Eng.*, **38**(5-6), 535-546.

https://doi.org/10.1016/j.compositesb.2006.06.016.

Guo, H., Cao, S., Yang, T. and Chen, Y. (2018), "Geometrically nonlinear analysis of laminated composite quadrilateral plates reinforced with graphene nanoplatelets using the element-free IMLS-Ritz method", *Compos. Part B Eng.*, **154**, 216-224. https://doi.org/10.1016/j.compositesb.2018.08.018.

Gudžulić, V., Dang, T.S. and Meschke, G. (2019), "Computational modeling of fiber flow during casting of fresh concrete", *Comput. Mech.*, **63**(6), 1111–1129. https://doi.org/10.1007/s00466-018-1639-9.

Guo, X., Liu, Y. and Wang, G. (2021), "Computer modeling for frequency performance of viscoelastic magneto-electro-elastic annular micro/nanosystem via adaptive tuned deep learning neural network optimization", *Adv. Nano. Res.*, **11**(2), 203-218. http://doi.org/10.12989/anr.2021.11.2.203.

Han, Z., Pan, E.and Zhang, Z. (2020), "Dynamic response of an embedded flexible foundation of general shape in a transversely isotropic and multilayered half-space", *Soil Dyn. Earthq. Eng.*, **139**, 106354. https://doi.org/10.1016/j.soildyn.2020.106354.

Hajmohammad, M.H., Nouri, A.H., Zarei, M.Sh. and Kolahchi, R. (2018), "A new numerical approach and visco-Sinusoidal shear deformation theory for blast analysis of auxetic honeycomb quadrilateral plates integrated by multiphase nanocomposite facesheets in hygrothermal environment", *Eng. Comput.*, **35**, 1141-1157. https://doi.org/10.1007/s00366-018-0655-x.

Hajmohammad, M.H., Zarei, M.Sh., Nouri, A. and Kolahchi, R. (2017), "Dynamic buckling of sensor/functionally graded-carbon nanotubes reinforced laminated quadrilateral plates/ actuator based on sinusoidal-visco piezoelasticity theories", *J. Sandw. Struct. Mat.*, In press, https://doi.org/10.1177/1099636217720373.

Huynh, H.D., Natarajan, S., Nguyen-Xuan, H. and Zhuang, X. (2020), "Polytopal composite finite elements for modeling concrete fracture based on nonlocal damage models", *Computat. Mech.*, **66**(6), 1257–1274. https://doi.org/10.1007/s00466-020-01898-y.

Kolahchi, R., Keshtegar, B. and Fakhar, M.H. (2018), "Optimization of dynamic buckling for sandwich nanocomposite quadrilateral plates with sensor and actuator layer based on sinusoidal visco-piezoelasticity theories using Grey Wolf algorithm". *J. Sandw. Struct. Mat.*, In press, https://doi.org/10.1177/1099636217731071.

Kolahchi, R., Zarei, M.S., Hajmohammad, M. H. and Nouri, A. (2017), "Wave propagation of embedded viscoelastic FG-CNT-reinforced sandwich quadrilateral plates integrated with sensor and actuator based on Sinusoidal shear deformation theory", *Int. J. Mech. Sci.*, **130**, 534-545. https://doi.org/10.1016/j.ijmecsci.2017.06.039.

Lee, M.G., An, J.H., Bae, S.G., Oh, H.S., Choi, J., Yun, D.Y., Hong, T., Lee, D.E. and Park, H.S. (2020), "Multi-objective sustainable design model for integrating CO_2 emissions and costs for slabs in office buildings", *Struct. Infrastruct. Eng.*, **16**(8), 1096-1105. https://doi.org/10.1080/15732479.2019.1683590.

Lee, M. and Kwak, H.G. (2021), "Numerical simulations of blast responses for SFRC slabs using an orthotropic model", *Eng. Struct.*, **238**, 112150. https://doi.org/10.1016/j.engstruct.2021.112150.

Loor, A.S., Rabani Bidgoli, M. and Mazaheri, H. (2021), "Optimization and buckling of rupture building beams reinforced by steel fibers on the basis of adaptive improved harmony search-harmonic differential quadrature methods", *Case Stud. Constr. Mater.*, **15**, e00647. https://doi.org/10.1016/j.cscm.2021.e00647.

Malveiro, J., Sousa, C., Ribeiro, D. And Calçada, R. (2018), "Impact of track irregularities and damping on the fatigue damage of a railway bridge deck slab", *Struct. Infrastruct. Eng.*, **14**(9), 1257-1268. https://doi.org/10.1080/15732479.2017.1418010.

Maalla, A. and Song, J. (2021), "Computational modeling for nonlinear magneto-electro-elastic responses of smart multi-phase symmetric system", *Adv. Nano. Res.*, **11**(3), 327-337. http://doi.org/10.12989/anr.2021.11.3.327.

Maheshwari, P. and Naramsetti, B.S. (2019), "Closed form solutions for response of machine foundations under accidental blast loads", *Soil Dyn. Earthq. Eng.*, **116**, 386-396. https://doi.org/10.1016/j.soildyn.2018.10.016.

Ragb, O., Matbuly, M.S. and Civalek, O. (2021), "Free vibration of irregular plates via indirect differential quadrature and singular convolution techniques", *Eng. Anal. Bound. Elem.*, **128**, 66-79. https://doi.org/10.1016/j.enganabound.2021.03.023.

Reifarth, C., Castedo, R., Santos, A.P., Chiquito, M., Lopez, L.M., Perez-Caldentey, A., Martinez-Almajano, S. and Alanon, A. (2021), "Numerical and experimental study of externally reinforced RC slabs using FRPs subjected to close-in blast loads", *Int. J. Impact Eng.*, **156**, 103939. https://doi.org/10.1016/j.ijimpeng.2021.103939.

Saheed, S., Arman, Y.H.M., El-Zeadani, M., Aziz, F.N.A., Fediuk, R., Alyousef, R. and Alabduljabbar, H. (2021), "Structural behavior of out-of-plane loaded precast lightweight EPS-foam concrete C-shaped slabs", *J. Build. Eng.*, **33**, 101597. https://doi.org/10.1016/j.jobe.2020.101597.

Shao, W. and Wu, X. (2011), "Fourier differential quadrature method for irregular thin plate bending problems on Winkler foundation", *Eng. Anal. Bound. Eleme.*, **35**(3), 389-394. https://doi.org/10.1155/2018/7476954.

Wu, J. and Chew, S.H. (2014), "Field performance and numerical modeling of multi-layer pavement system subject to blast load", *Constr. Build. Mater.*, **52**, 177-188. https://doi.org/10.1016/j.conbuildmat.2013.11.035.

Yang, J., Zhu, S. and Zhai, W. (2020), "A novel dynamics model for railway ballastless track with medium-thick slabs", *Appl. Math. Model.*, **78**, 907-931. https://doi.org/10.1016/j.apm.2019.09.051.

Zhang, Y.X., Bradford, M.A. and Gilbert, R.I. (2007), "A layered cylindrical quadrilateral shell element for nonlinear analysis of RC plate structures", *Adv. Eng. Softw.*, **38**(7), 488-500. https://doi.org/10.1016/j.advengsoft.2006.09.017.

Zhang, L.W. (2017), "The IMLS-Ritz analysis of laminated CNT-reinforced composite quadrilateral plates subjected to a sudden transverse dynamic load", *Compos. Struct.*, **180**, 638-646. https://doi.org/10.1016/j.compstruct.2017.07.046.

Zhao, C., Ye, X., He, K. and Gautam, A. (2020), "Numerical study and theoretical analysis on blast resistance of fabricated concrete slab", *J. Build. Eng.*, **32**, 101760. https://doi.org/10.1016/j.jobe.2020.101760.

AT

Appendix

$$K = K_{out}\left[1+\frac{\xi\left(\frac{K_{in}}{K_{out}}-1\right)}{1+\alpha(1-\xi)\left(\frac{K_{in}}{K_{out}}-1\right)}\right] \quad , \tag{A1}$$

$$G = G_{out}\left[1+\frac{\xi\left(\frac{G_{in}}{G_{out}}-1\right)}{1+\beta(1-\xi)\left(\frac{G_{in}}{G_{out}}-1\right)}\right], \tag{A2}$$

where

$$K_{in} = K_m + \frac{(\delta_r - 3K_m\chi_r)C_r\zeta}{3(\xi - C_r\zeta + C_r\zeta\chi_r)}, \tag{A3}$$

$$K_{out} = K_m + \frac{C_r(\delta_r - 3K_m\chi_r)(1-\zeta)}{3[1-\xi-C_r(1-\zeta)+C_r\chi_r(1-\zeta)]}, \tag{A4}$$

$$G_{in} = G_m + \frac{(\eta_r - 3G_m\beta_r)C_r\zeta}{2(\xi - C_r\zeta + C_r\zeta\beta_r)}, \tag{A5}$$

$$G_{out} = G_m + \frac{C_r(\eta_r - 3G_m\beta_r)(1-\zeta)}{2[1-\xi-C_r(1-\zeta)+C_r\beta_r(1-\zeta)]}, \tag{A6}$$

where $\chi_r, \beta_r, \delta_r, \eta_r$ may be calculated as

$$\chi_r = \frac{3(K_m+G_m)+k_r-l_r}{3(k_r+G_m)}, \tag{A7}$$

$$\beta_r = \frac{1}{5}\left\{\begin{matrix}\frac{4G_m+2k_r+l_r}{3(k_r+G_m)}+\frac{4G_m}{(p_r+G_m)} \\ +\frac{2[G_m(3K_m+G_m)+G_m(3K_m+7G_m)]}{G_m(3K_m+G_m)+m_r(3K_m+7G_m)}\end{matrix}\right\}, \tag{A8}$$

$$\delta_r = \frac{1}{3}\left[n_r+2l_r+\frac{(2k_r-l_r)(3K_m+2G_m-l_r)}{k_r+G_m}\right], \tag{A9}$$

$$\eta_r = \frac{1}{5}\left[\begin{matrix}\frac{2}{3}(n_r-l_r)+\frac{4G_mp_r}{(p_r+G_m)} \\ +\frac{8G_mm_r(3K_m+4G_m)}{3K_m(m_r+G_m)+G_m(7m_r+G_m)} \\ +\frac{2(k_r-l_r)(2G_m+l_r)}{3(k_r+G_m)}\end{matrix}\right]. \tag{A10}$$

where, K_m and G_m are the bulk and shear moduli of the matrix which can be written as

$$K_m = \frac{E_m}{3(1-2\upsilon_m)} \quad , \tag{A11}$$

$$G_m = \frac{E_m}{2(1+\upsilon_m)}. \tag{A12}$$

Furthermore, β, α can be obtained from

$$\alpha = \frac{(1+\upsilon_{out})}{3(1-\upsilon_{out})} \quad , \tag{A13}$$

$$\beta = \frac{2(4-5\upsilon_{out})}{15(1-\upsilon_{out})}, \tag{A14}$$

$$\upsilon_{out} = \frac{3K_{out}-2G_{out}}{6K_{out}+2G_{out}}. \tag{A15}$$

where two parameters ξ and ζ show the agglomeration of CNFs as

$$\xi = \frac{V_{inclusion}}{V}, \tag{A16}$$

$$\zeta = \frac{V_r^{inclusion}}{V_r}. \tag{A17}$$

However, the average volume fraction c_r of CNFs in the NFRP is

$$C_r = \frac{V_r}{V}. \tag{A18}$$